Role of paramagnetic defects in light emission processes in Y-doped ZrO$_2$ nanopowders

Role of paramagnetic defects in light emission processes in Y-doped ZrO$_2$ nanopowders

N Korsunska[1], M Baran[1], A Zhuk[1], Yu Polishchuk[1], T Stara[1], V Kladko[1], Yu Bacherikov[1], Ye Venger[1], T Konstantinova[2] and L Khomenkova[1]

[1] V. Lashkaryov Institute of Semiconductor Physics of the National Academy of Sciences of Ukraine, 45 Pr. Nauky, Kyiv 03028, Ukraine
[2] Donetsk Institute for Physics and Engineering, named after O.O. Galkin of the National Academy of Sciences of Ukraine, 72 R. Luxemburg str., Donetsk 83114, Ukraine
E-mail: kors@isp.kiev.ua and khomen@ukr.net

Abstract

Luminescence and structural properties of pure and Y-doped ZrO$_2$ nanopowders with different Y content synthesized by co-precipitation of Zr and Y salts were investigated by x-ray diffraction, transmission electron microscopy, electron paramagnetic resonance (EPR) and photoluminescence (PL) methods. It was found that at constant calcination temperature (700 °C), the increase of Y content stimulates the transformation of crystalline phase from monoclinic through the tetragonal to the cubic one. Generally, room temperature PL emission was found to be similar for the samples with different Y content, demonstrating the same overlapped PL components in visible spectral range under extrinsic excitation. The relative contribution of each PL component was found to be affected by calcination time. In EPR spectra of as-prepared samples no signals were observed. The annealing in N$_2$ or H$_2$ flow results in the appearance of the signal from surface Zr^{3+} defects. In the latter the signal assigned to F-center also arises. The anti-correlation observed between the PL intensity and the value of the Zr^{3+} EPR signal allows us to conclude that the Zr^{3+} center is the center of fast non-radiative recombination. At the same time, interrelation between the intensity of the EPR signal assigned to F-centers and observed PL bands was not found.

S Online supplementary data available from stacks.iop.org/MRX/1/045011/mmedia

Keywords: zirconium oxide, photoluminescence, defects, Y-doping, electron paramagnetic resonance, x-ray diffraction, transmission electron microscopy

1. Introduction

Zirconia (ZrO_2) has attracted considerable attention because of its mechanical, electric, thermal and luminescent properties. Emitting ZrO_2 enables different applications, for example, functional, structural and medical applications, solid oxide fuel cells, oxygen sensor [1, 2], laser techniques, thermo-luminescent UV dosimeters [3], biological labeling [4], etc. Different defect-related emission bands in visible spectral range can be observed in pure and/or Y-doped ZrO_2 (YZO) materials [5, 6] that also offer an application of zirconia for light-emitting devices. In particular, either several overlapped emission bands or single featureless broad band, whose intensity and peak position depended on excitation wavelength, were observed in photoluminescence (PL) spectra of pure or YZO at $300\,K$ [5–8]. This emission originates from defect states [5, 7–9] and it is usually attributed to intrinsic defects of ZrO_2: oxygen vacancies or their complexes located in the crystal volume [5, 10] as well as oxygen vacancies located at grain surface [7] or near impurities [5] (for example, near Y ions stabilized tetragonal ZrO_2 structures). In addition, T-defect (Zr^{3+} in the bulk of crystal [11] or unsaturated Zr sites at crystal surface (surface Zr^{3+} [12]) and the distortion of lattice by oxygen vacancies [8] were considered as emitting sources. For example, blue band (460 nm) was attributed to intradefect transition in F^+-centers, while green–orange bands (550 nm and 600 nm) were ascribed to Y-contained complexes [5]. At the same time in [7] the emission band at 450 nm was attributed to bulk vacancies that appeared due to the presence of Y ions, while the band at 570 nm was associated with the localized states at the grain boundaries or at the grain surface.

The variety of emission bands is determined by the variety of structural defects. This can explain the observation of the abundance of emission bands whose peak positions depend on crystallite size [7], doping and preparation technique [8, 13, 14]. Furthermore, the shift of PL peak position with the change of excitation wavelength [5, 8, 15] is obviously caused by the overlapping of different PL bands. Besides the different models of emitting centers, different radiative transitions (the intradefect transition [5, 15] or radiative recombination of photogenerated hole [11]) were considered to explain luminescence bands.

To clarify the nature of emission centers, annealing in different atmospheres, which affects the oxygen vacancies content, was used. However, different data were obtained. For example, annealing of ZrO_2 nanocrystals in an oxygen–nitrogen gas mixture with low oxygen partial pressure (when formation of oxygen vacancies can be expected) showed that upon such treatment the variation of PL intensity depends on excitation wavelength [8]. It was found that under excitation within the band gap, PL intensity increased and this was ascribed to the increase of oxygen vacancies content. However, under band-to-band excitation a decrease of PL intensity was observed. On the other hand, the enhancement of PL intensity under excitation within the band gap was revealed for ZrO_2 thin films annealed in O_2 atmosphere (when the decrease of oxygen vacancy content has to be expected) [16]. This effect was ascribed to reconstruction of ZrO_2 nanocrystals interfaces, which results in passivation of the non-radiative defects or stress relaxation. Thus, the different processes can affect the variation of the PL spectra. Furthermore, the nature of emitting and non-radiative centers and the mechanisms of oxygen influence are not clear yet. Meanwhile, the F-centers as well as bulk and surface Zr^{3+}-centers can be observed in electron paramagnetic resonance (EPR) spectra [11, 12, 17–19]. Therefore, comparison of the variation of their concentration with the transformation of PL spectra can give additional information about the origin of emission bands. However, only a few investigations have been devoted to such a comparison [10].

In the present work the PL and EPR spectra as well as structural properties of ZrO_2-based nanopowders with different Y content were investigated. In addition, the influence of an annealing atmosphere on PL and EPR spectra was studied, aiming to control intrinsic defects.

2. Methods

Pure and YZO nanopowders (with Y content of 10 and 15 at%) were synthesized by a co-precipitation technique using $ZrOCl_2 \cdot nH_2O$ and $Y(NO_3)_3 \cdot nH_2O$ salts. The 25% NH_4OH water solution was used as the precipitant. Sediments were mixed for 1 h at room temperature at pH = 9. After this, they were repeatedly washed, filtered with distilled water and then the hydrogel was dried in a microwave furnace and calcined at 700 °C. More details can be found elsewhere [20, 21]. The calcination time was 1 h for pure ZrO_2 and for YZO with 15 at% of Y (abbreviated as ZYO-15), whereas for samples with 10 at% it was 1 h (ZYO-10-1) and 2 h (ZYO-10-2).

To modify the defect content in the samples, an additional thermal treatment was performed at 800 °C for 2 h in the N_2 flow or at 350 °C for 30 min in H_2 flow.

Elemental analysis of pure and YZO powders was performed by means of the x-ray fluorescent method using EXPERT 3L W144U setup. Relative mass contribution of single elements such as ^8O, ^{39}Y and ^{40}Zr was detected and corresponding molar concentration was extracted.

The structural properties were investigated by means of x-ray diffraction (XRD) and transmission electron microscopy (TEM) methods. XRD data were collected in the range of $2\theta = 20$–$80°$ using an ARL X'TRA powder diffractometer with CuK_α wavelength ($\lambda = 0.15\,418$ nm) and grazing geometry (the angle of incident beam was $\omega \sim 0.5°$). TEM observation was performed with a JEOL JEM 200A instrument using the carbon-replica technique. More details can be found elsewhere [22]. It worth noting that both XRD and TEM methods are suitable for the estimation of grain sizes for the samples produced at 700 °C (figure 1S, supplemented data, available at stacks.iop.org/MRX/1/045011/mmedia).

PL was excited by 337 nm light of an N_2-laser and recorded using an SDL-2 system coupled with a photomultiplier tube. EPR spectra were measured using a Varian-12 spectrometer. The modulation frequency was 100 kHz and the modulation amplitude was 0.1–0.2 mT. All measurements were performed at room temperature.

3. Results

3.1. Structural properties

The XRD patterns of pure and YZO powders show several peaks corresponding to different ZrO_2 crystallographic planes (figure 1(a)). The peak assignment to the relevant crystalline phase (monoclinic, tetragonal or cubic) was based on comparison with tabled XRD data [23]. This allowed not only the identification of the type of lattice, but also the estimation of the sample composition.

The XRD pattern of pure ZrO_2 (figure 1(a), curve 1) shows its monoclinic structure [23]. The ZYO-10-1 and ZYO-10-2 samples demonstrate the reflections at $2\theta \sim 30.3°$, 35.0°, 43.2°, 50.5°, 59.6°, 62.8° (figure 1(a), curves 2,3). Furthermore, in the range of $2\theta = 72$–$75°$ an asymmetric broad peak at $2\theta \sim 74.2°$ from (400) family planes is observed for the ZYO-10-1
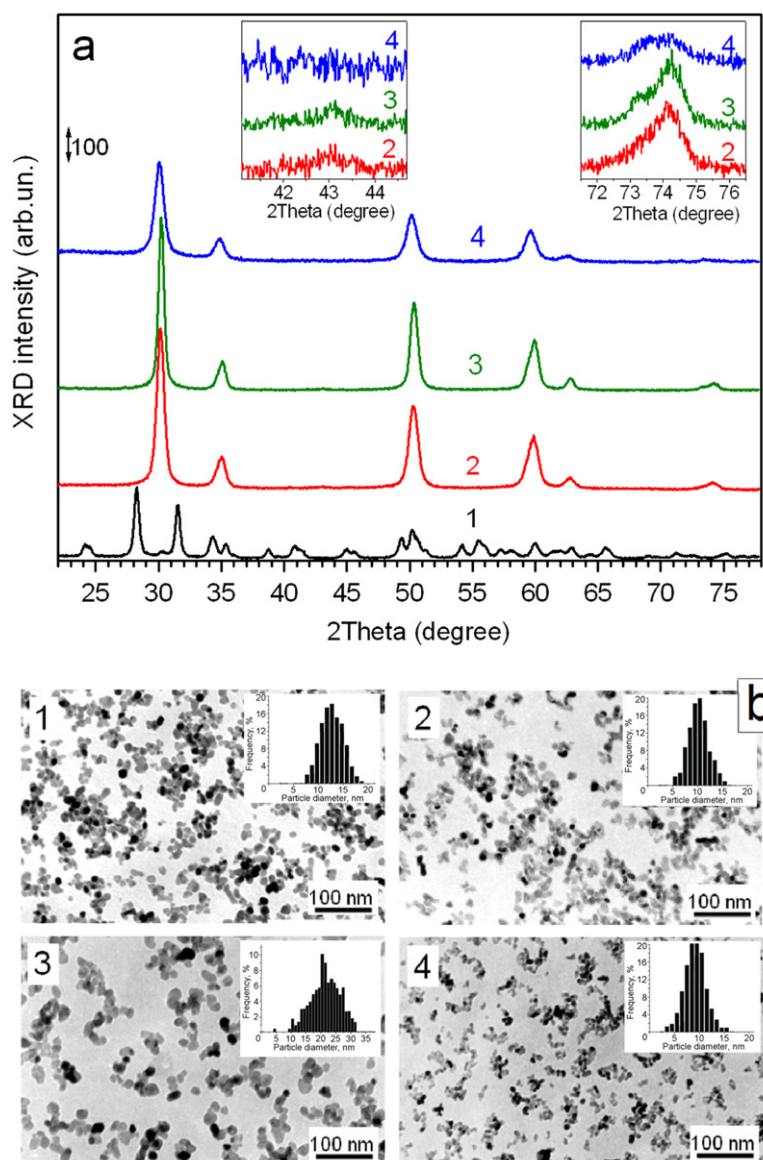
Figure 1. (a) XRD patterns of pure ZrO_2 (1) and ZYO powders with different Y_2O_3 content −10 at% (2,3) and 15 at% (4). The insets demonstrate in detail the reflections from (102) and (004) planes for ZYO powders. b) Bright-field TEM images of pure ZrO_2 (1) and ZYO powders with different Y_2O_3 content: 10 at% (2,3) and 15 at% (4). The grain size distribution is presented for each powder in corresponding insets.

sample (figure 1(a) and inset, curve 2), as well as a doublet at $2\theta \sim 73.2°$ from (004) plane, and $2\theta \sim 74.2°$ (400) is detected for ZYO-10-2 powder (figure 1(a) and inset, curve 3). All XRD peaks for the ZYO-10-1 sample are broader than those for ZYO-10-2. It worth noting that in the case of the ZYO-10-1 sample the asymmetric shape of the peak at $2\theta \sim 74.2°$ suggests that it is the superposition of at least two peaks. One of them obviously reaches a peak at $2\theta \sim 74.2°$, while it can be supposed that another peak corresponds to the reflection at $2\theta \sim 73.2°$. The lower resolution of these peaks in ZYO-10-1 powder compared with the ZYO-10-2 sample can originate from the higher width of XRD reflections resulting in higher overlapping of the peaks

at $2\theta \sim 73.2°$ and $74.2°$. Another reason can be the lower intensity of the peak at $2\theta \sim 73.2°$ that can be connected with some deterioration of ZYO-10-1 grain structure or with the difference in grain shape. The peak at $2\theta \sim 43.2°$ (102) and the doublet at $2\theta \sim 73.2°$ and $74.3°$ (figure 1(a), insets) are the features of tetragonal phase [23]. The analysis of XRD data also allowed the estimation of the Y content in the powders based on tabled XRD data [23]. It was found that the samples calcinated during 1 h and 2 h had a similar composition and the Y content was nearly 9.5 at%, which was close to the results of elemental analysis (10 at%).

The ZYO-15 sample shows the presence of the peaks at $2\theta \sim 30.0°$, $34.8°$, $50.5°$, $59.6°$, $62.8°$ and $73.8°$ (figures 1(a), 3). The absence of the peak at $2\theta \sim 43.2°$ testifies to the presence of the cubic phase, but the broad peak at $2\theta \sim 73.8°$ can be caused by the superposition of the reflections from cubic and tetragonal ones. Thus, the structure of sample ZYO-15 can be considered as the superposition of cubic and tetragonal phases [23] with preferable contribution of the former one (figure 1(a), insets). The Y content estimated from XRD data for this sample is ~ 15 at%, which coincides with the data of elemental analysis.

It is worth noting that all these XRD peaks detected for ZYO-15 powder are broader than those observed for ZYO-10-1 powder. Taking into account that the broadening of Bragg peaks is due to pure size effects, mean grain size, d, was directly deduced from the full width at half maximum (β_{hkl}) of the peaks. The sizes of nanocrystals were estimated from different reflections using the classical Scherrer equation $d_{hkl} = 0.9 \cdot \lambda/(\beta_{hkl} \cdot \cos\theta)$. For the same sample different d values were obtained from different XRD peaks that reflect a non-spherical shape of nanocrystals. This difference was most pronounced for pure ZrO_2, which could be caused by the specific character of monoclinic phase growth [20].

The sizes of nanocrystals were found to be $d = 12.6 \pm 2.6$ nm for the pure ZrO_2 sample, $d = 10.9 \pm 1.0$ nm for the ZYO-10-1 sample and $d = 20.0 \pm 1.0$ nm for the ZYO-10-2 sample as well as $d = 9.9 \pm 1.0$ nm for the ZYO-15 sample. Thus, the increase of Y content stimulates the decrease of nanocrystal sizes. At the same time, the increase of calcination time results in their enlargement, which is in agreement with the results obtained previously for the YZO samples presented in figure 2S (see supplemented data).

TEM observation was performed for the same powders, and corresponding bright-field TEM images are shown in figure 1(b). It can be seen that the powders obtained by the co-precipitation technique are single crystals with soft and easily destroyed agglomerates, which is important for their successful application. The analysis of crystal size from TEM images was performed. The results were found to be close to the data of the XRD experiment for the samples investigated.

3.2. Light-emitting properties

3.2.1. As-prepared samples.
PL spectra of pure ZrO_2 and ZYO samples are shown in figure 2(a). The spectra contain wide structural bands in the region of 2.25–3.10 eV (400–550 nm) and the shoulder in the range of 2.06–2.17 eV (570–600 nm). The observed PL band can be approximated by three Gaussian-like components with maxima positions at ~ 2.81 eV (440 nm), ~ 2.43 eV (510 nm) and ~ 2.11 eV (587 nm) (figure 2(b)).

The PL intensity did not vary considerably in all the samples investigated (figure 2(b)). Besides, the PL peak position depends slightly on Y content in the samples calcinated during 1 h (figure 2(a)). At the same time the increase of calcination time up to 2 h results in the blue shift of PL peak position (figure 2(a), curve 4). This is obviously caused by the increase of the
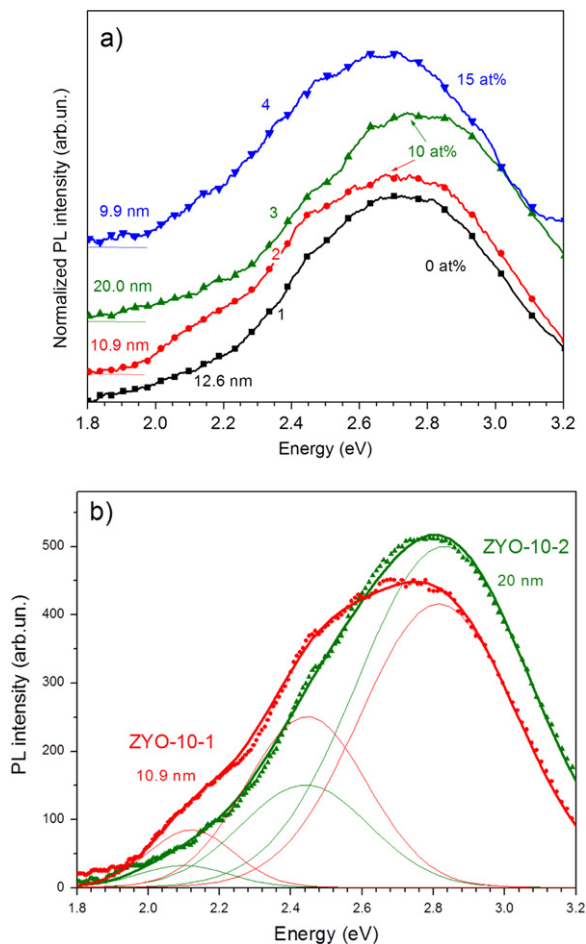
Figure 2. (a) PL spectra of pure ZrO_2 (1) and ZYO powders with 10 at% (2,3) and 15 at% (4) of Y. The calcination times are 1 h (1,2,4) and 2 h (3). b) Deconvolution of PL spectra of YZO powder with 10 at% of Y presented in figure 2(a) by the curves 2 and 3.

contribution of the 2.81 eV PL component and by the decrease of the intensities of the 2.11 and 2.43 eV PL components (figure 2(b)). Thus, the contribution of the last two components is more pronounced in the samples with small grain size.

3.2.2. Influence of annealing. An investigation into the effect of thermal treatment in an oxygen-lacking atmosphere, usually used for intrinsic defect formation, on PL and EPR spectra, was performed for the ZYO-10-2 sample.

PL spectra measured before and after annealing at 800 °C in N_2 flow are presented in figure 3(a). It is seen that the main effect of annealing is the decrease of total PL intensity. Furthermore, the decrease of 2.11 eV PL component is evidently more pronounced (figure 3(a)). After an annealing in H_2 flow, the effect of the PL intensity decrease, including the change of 2.11 eV PL component contribution, is more apparent (figure 3(b)). After storage at room temperature in air, the PL intensity of the sample annealed in H_2 increases and the shape of the PL spectrum is gradually restored (figure 3(b), curve 3).
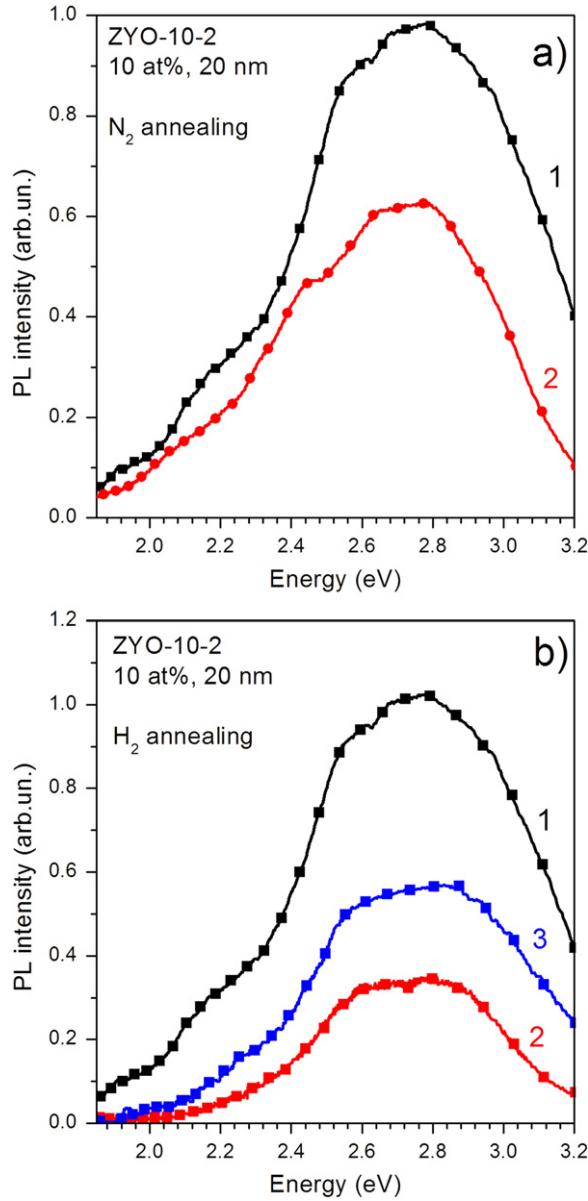
Figure 3. PL spectra of ZYO-10-2 powder annealed in nitrogen (a) and hydrogen (b) atmosphere measured at 300 K. $\lambda_{exc} = 337$ nm. (1) – before annealing, (2) – after annealing, (3) – after 2 weeks' storage in ambient air at 300 K.

3.3. EPR spectra

For all as-prepared samples, no EPR signals were observed (only the signal from Cr^{3+}-MgO reference was detected (figure 4(a), curve 1)), but thermal treatment results in the appearance of EPR signals. The influence of annealing in an oxygen-lacking atmosphere was investigated mainly for the ZYO-10-2 powder, whose PL spectra were presented above.

After annealing in N_2 flow, the anisotropic signal with $g_{\perp} = 1.975$ and $g_{\parallel} = 1.958$ arises (figure 4(a), curve 2). This signal was earlier assigned to Zr^{3+} at the crystal surface [12, 17–19]. After annealing in H_2 flow, the surface Zr^{3+} signal also appears (figure 4(a), curve 3), but its
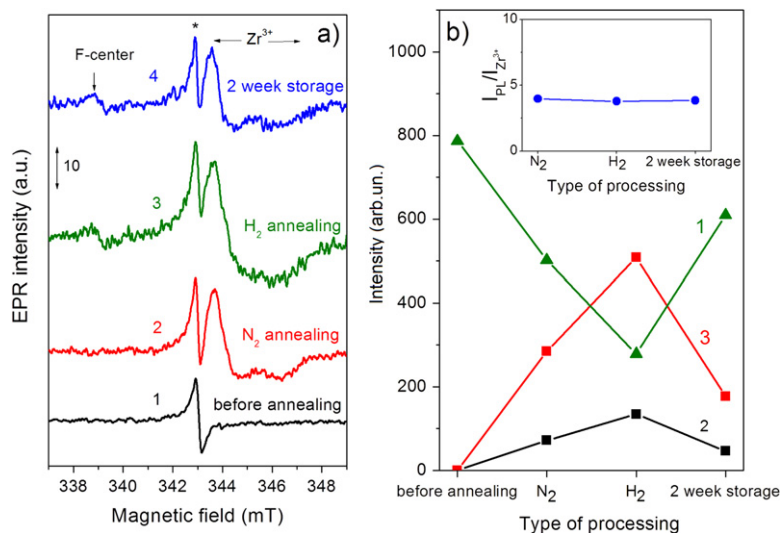
Figure 4. (a) Evolution of EPR spectra of ZYO-10-2 powder (1) under thermal treatment in a nitrogen (2) and hydrogen (3) atmosphere as well as after 2 weeks' storage in ambient air at 300 K (4). The signal from the Cr^{3+}-MgO replica is marked at the top, next to the star. b) Variation of integrated values of PL intensity (1) and the Zr^{3+} EPR signal (2) upon different types of processing. The inset represents the ratio of difference between integrated PL intensities before and after each treatment (ΔI_{PL}, curve 3) to the integrated intensity of the Zr^{3+} EPR signal upon corresponding treatment ($I_{Zr^{3+}}$, curve 2).

intensity is higher than in the previous case (figure 4(b)). In addition, the signal with $g = 2.003$ assigned to the F-center [19] was also observed (figure 4(a), curve 3). Storage of annealed samples for several weeks in air leads to the decrease of the intensity of the Zr^{3+}-related signal, whereas the intensity of the EPR signal from the F^+-center practically does not change (figure 4).

4. Discussion

As figure 2 shows, the PL spectra of all the samples investigated were recorded under the excitation below the band gap and consisted of several overlapped PL bands. This finding is similar to other observations of pure and Y-stabilized ZrO_2 [5–10]. They were attributed to different intrinsic defects such as oxygen vacancies, Zr^{3+} centers, etc. These different PL bands can be excited by the same monochromatic light due to the fact that corresponding absorption bands, related to intrinsic defects, extend from 300 to 700 nm and overlap [11, 24]. Our excitation wavelength (337 nm) lies within this interval, which allows different emitting centers to be excited. Therefore, the changes in their concentration due to external action (annealing) or due to changes in Y content and nanocrystal sizes have to result in changes in PL spectra shape.

We did not observe significant changes of PL spectra shape with the changes of Y content, which shows the presence of the same defects with nearly the same concentration, in our samples calcined for 1 h. Furthermore, the increase of calcination time, resulting in an increase of crystallite sizes, leads to a change in the redistribution of PL component intensities. The formation of larger grains is accompanied by the decrease of their surface/volume ratio. This

can be the reason for the blue-shift of PL peak position caused by the increase of the contribution of the 2.81 eV PL component and the decrease in intensity of the 2.11 eV and 2.43 eV PL components. Thus, one can ascribe the 2.8 eV PL component to the volume defects. This is in an agreement with the conclusion of Ref. [7], where similar PL emission was also attributed to grain volume defects (F-center). At the same time, the 2.11 and 2.43 eV PL components are more pronounced for the samples with smaller grains (figure 2(a)), which allows attributing them to the grain surface defects. This is in accordance with the data of Ref. [7] where the 2.17 eV PL component which is close to that observed in our spectra (figure 2) was ascribed to defect states at the grain boundaries [7]. At the same time, the PL band that peaked near 2.4 eV was attributed to volume Zr^{3+} defect (T-center) [11]. On the other hand, the surface Zr^{3+} center was also considered as an emission center [6].

Both F-centers and Zr^{3+} defects manifest themselves in EPR spectra, and their concentration can be changed by the annealing in a nitrogen and/or hydrogen atmosphere.

It was supposed that an annealing in a N_2 or even a N_2–O_2 gas mixture with low O_2 content must result in the formation of oxygen vacancies [8]. However, in our case the appearance of a surface Zr^{3+} EPR signal was only observed after annealing in a N_2 atmosphere (figure 4(a)).

It is known that an annealing in a H_2 atmosphere produces F-centers [17, 19] and surface Zr^{3+} defects [17]. Indeed, in our samples the appearance of these centers was observed (figure 4(a)). It should be noted that the signal from surface Zr^{3+} centers differs from the signal corresponding to volume Zr^{3+} ones (T-defects), which was associated with the absorption band at 3.3 eV and the PL band at 2.47 eV [11]. This EPR signal was not observed in our samples in spite of the presence of such a PL component.

The variation of integrated EPR and PL intensities with different processing (annealing, storage in air) is present in figure 4(b). The main effect of both types of annealing is seen as the decrease of PL intensity accompanied by the appearance of EPR centers. After sample storage in air, the PL intensity recovers (figure 4(b), curve 1), whereas the Zr^{3+} EPR signal decreases (figure 4). Since the EPR signal from the F-centers either did not change after storage (for the samples annealed in H_2) or was not detected (for the powders annealed in N_2), we can conclude that the variation of PL intensity is caused by the variation of the Zr^{3+} defect number. This is confirmed by the anti-correlation of the variation of PL intensity (figure 4(b), curve 1) and Zr^{3+} EPR signal (curve 2). As one can see from the inset of figure 4(b), the ratio $R = \Delta I_{PL}/I_{Zr^{3+}}$, where the ΔI_{PL} is the difference between integrated PL intensities before and after each treatment and the $I_{Zr^{3+}}$ is the intensity of the Zr^{3+} EPR signal at the corresponding treatment, is constant whatever the processing (i.e. the change in integrated PL intensity is proportional to the change in the EPR signal). Thus, one can consider surface Zr^{3+} centers as the centers of fast non-radiative recombination.

It should be noted that the appearance of such centers has to decrease all the PL components proportionally. However, the 2.11 eV PL component showed a more pronounced decrease upon annealing in H_2 flow and recovered well after storage in air. Thus one can assume that the variation of its intensity is caused not only by Zr^{3+} variation, but also by variation in the concentration of corresponding emitting centers. In this case, the unchanged R values can be explained by the low contribution of the 2.11 eV PL component to PL spectra. Furthermore, its recovery testifies to the surface nature of corresponding emitting centers. This is in agreement with the conclusion obtained from the analysis of the influence of grain sizes on PL spectra.

The formation of surface Zr^{3+} centers during annealing can be caused either by desorption of some species from crystal surfaces or by formation of surface oxygen vacancies [9]. Both these processes can stimulate the appearance of Zr^{3+} centers upon annealing in a H_2 atmosphere. At the same time, upon annealing in N_2 flow, when an appearance of F-centers was not observed, the desorption of some surface species can mainly contribute the formation of Zr^{3+} centers. The decrease of Zr^{3+} content and the increase of PL intensity during storage in air are obviously due to the passivation processes or the healing of the surface oxygen vacancies.

It should be pointed out that the effect of the surface Zr^{3+} center on PL spectra of the powders should depend on the grain sizes as well as on the excitation light wavelength. In the small crystals the influence of Zr^{3+} -centers on PL intensity have to be observed both under extrinsic and intrinsic excitation. In the case of crystallites with sizes that exceed the value of region of band-to-band light absorption, the decrease of PL intensity can be observed mainly under the excitation above the band gap. This can be the reason for the difference in the effect of annealing in an oxygen-free or an oxygen atmosphere as observed in different papers.

In contrast to observed Zr^{3+} centers, the F-centers are obviously volume-related defects since the intensity of the corresponding EPR signal does not change during storage. This center in the crystal volume is usually associated with the PL band peaking at 2.6–2.8 eV [10]. However, no correlation was observed in our samples between a specific PL component and the EPR signal from F-centers, whatever the processing. One could suppose that another PL band (in particular in the UV spectral region, which was not scanned in our experiments) is connected with the F-center.

5. Conclusions

Luminescence and structural properties of pure and YZO nanopowders with different Y content were investigated. It was found that at constant calcination temperature, the increase of Y content stimulates the transformation of the crystalline phase from monoclinic through tetragonal to cubic as well as the decrease of nanocrystal sizes. The size value estimated from different XRD peaks reflects the anisotropic character of crystal growth (it is more pronounced for the monoclinic phase). Room temperature PL spectra of the samples with different Y content under extrinsic excitation consist of several overlapped bands (at 2.11 eV, 2.43 eV and 2.81 eV), being the same for the samples with different Y content. The increase of the intensity of 2.11 eV and 2.43 eV PL components is more pronounced for the smaller nanocrystals, whereas the contribution of the 2.81 eV PL component is more considerable for larger grains. It was concluded that the former PL components are surface related, while the latter is connected with volume defects. No signals were detected in EPR spectra of as-prepared samples. Their annealing in N_2 or H_2 flow results in the appearance of the signal from surface Zr^{3+} defects. In the last case the signal assigned to the F-center also arises. The observed anti-correlation between PL intensity and the intensity of the EPR signal from Zr^{3+} testifies that this center is the center of fast non-radiative recombination. At the same time no correlation between the intensity of the signal assigned to F-centers and observed PL bands was found.

References

[1] Fidelus J D, Łojkowski W, Millers D, Grigorjeva L, Smits K and Piticescu R R 2007 Zirconia based nanomaterials for oxygen sensors—generation, characterisation and optical properties *Solid State Phenom.* **128** 141–50

[2] Fidelus J D, Lojkowski W, Millers D, Smits K and Grigorjeva L 2009 Advanced nanocrystalline ZrO_2 for optical oxygen sensors *IEEE Sensors* **9** 1268–72

[3] Ken Yueh H and Cox B 2003 Luminescence properties of zirconium oxide films *J. Nucl. Mater.* **323** 57–67

[4] Jia R, Yang W, Bai Y and Li T 2004 Upconversion photoluminescence of $ZrO_2:Er^{3+}$ nanocrystals synthesized by using butadinol as high boiling point solvent *Opt. Mater.* **28** 246–9

[5] Petrik N G, Tailor D P and Orlando T M 1999 Laser-stimulated luminescence of yttria-stabilized cubic zirconia crystals *J. Appl. Phys.* **85** 6770–6

[6] Anpo M, Nomura T, Kondo J, Domen K, Maruya K I and Onishi T 1990 Photoluminescence and FT-IR studies of the dissociative adsorption of H_2 on the active ZrO_2 catalyst and its role in the hydrogenation of CO *Res. Chem. Intermediate* **13** 195–202

[7] Nakajima H and Mori T 2006 Photoluminescence excitation bands corresponding to defect states due to oxygen vacancies in yttria-stabilized zirconia *J. Alloys Compd.* **408–412** 728–31

[8] Smits K, Grigorjeva L, Millers D, Sarakovskis A, Grabis J and Lojkowski W 2011 Intrinsic defect related luminescence in ZrO_2 *J. Lumin.* **131** 2058–62

[9] Lakshmi J S, John Berlin I, Daniel G P, Thomas P V and Joy K 2011 Effect of calcination atmosphere on photoluminescence properties of nanocrystalline ZrO_2 thin films prepared by sol–gel dip coating method *Physica* B **406** 3050–5

[10] Lin C, Zhang C and Lin J 2007 Phase transformation and photoluminescence properties of nanocrystalline ZrO_2 powders prepared via the pechini-type sol–gel process *J. Phys. Chem.* C **111** 3300–7

[11] Orera V M, Merino R I, Chen Y, Cases R and Alonso P J 1990 Intrinsic electron and hole defects in stabilized zirconia single crystals *Phys. Rev.* B **42** 9782–9

[12] Jacob K H, Knozinger E and Benfer S 1994 Chemisorption of H_2 and H_2-O_2 on polymorphic zirconia *J. Chem. Soc, Faraday Trans.* **90** 2969–75

[13] Smits K, Millers D, Grigorjeva L, Fidelus J D and Lojkowski W 2007 Comparison of ZrO_2:Y nanocrystals and macroscopic single crystal luminescence *J. Phys.: Conf. Ser.* **93** 012035

[14] Li Q, Ai D, Dai X and Wang J 2003 Photoluminescence of nanometer zirconia powders *Powder Technol.* **137** 34–40

[15] Korsunska N, Papusha V, Kolomys O, Strelchuk V, Kuchuk A, Kladko V, Yu B, Konstantinova T and Khomenkova L 2014 Nanostructured Y-doped ZrO_2 powder: peculiarities of light emission under electron beam excitation *Phys. Status Solidi* C **11** 1417–22

[16] John Berlin I, Anitha V S, Thomas P V and Joy K 2012 Influence of oxygen atmosphere on the photoluminescence properties of sol–gel derived ZrO_2 thin films *J. Sol.-Gel Sci. Technol.* **64** 289–96

[17] Zhao Q, Wang X and Cai T 2004 The study of surface properties of ZrO_2 *Appl. Surf. Sci.* **225** 7–13

[18] Wright S and Barklie R C 2006 EPR characterization of defects in monoclinic powders of ZrO_2 and HfO_2 *Mat. Sci. Semicond. Proc.* **9** 892–6

[19] Frolova E V and Ivanovskaya M I 2006 The origin of defects formation in nanosized zirconia *Mat. Sci. Eng.* C **26** 1106–10

[20] Konstantinova T, Danilenko I, Glazunova V, Volkova G and Gorban O 2011 Mesoscopic phenomena in oxide nanoparticles systems: processes of growth *J. Nanoparticle Res.* **13** 4015–23

[21] Konstantinova T, Danilenko I and Varyukhin V 2013 Effects of surface and interface in oxide nanoparticle system in *Nanomaterials Imaging Techniques, Surface Studies, and Applications, Proc. FP7 Int. Summer School Nanotechnology: from Fundamental Research to Innovations (Bukovel, Ukraine, 26 August–2 September 2012)* ed O Fesenko, L Yatsenko and M Brodin *Springer Proceedings in Physics* **146** 135–44

[22] Doroshkevich A S, Danilenko I A, Konstantinova T E, Volkova G K and Glazunova V A 2010 Structural evolution of zirconia nanopowders as a coagulation process *Crystallogr. Rep.* **55** 863–5

[23] Powder Diffraction Files, Cards No. 000-07-343, 010-82-1242, 000-30-1468, 000-60-0504, PDF-2 Database of International Centre for Diffraction Data (ICDD), Newton Square, PA 19073-3273, USA, release 2012

[24] Costantini J-M and Beuneum F 2011 Point defects induced in yttria-stabilized zirconia by electron and swift heavy ion irradiations *J. Phys.: Condens. Matter* **23** 115902